Article

On the Aromaticity and ^{13}C-NMR Pattern of Pentagonal-Pyramidal Hexamethylbenzene Dication [C$_6$(CH$_3$)$_6$]$^{2+}$: A {C$_5$(CH$_3$)$_5$}$^−$–{CCH$_3$}$^{3+}$ Aggregate

Desmond MacLeod-Carey [iD] **and Alvaro Muñoz-Castro** *

Laboratorio de Química Inorgánica y Materiales Moleculares, Universidad Autónoma de Chile, Llano Subercaceaux 2801, San Miguel, Santiago 8900000, Chile; desmond.macleod@uautonoma.cl
* Correspondence: armunozc@gmail.com

Abstract: The experimentally characterized hexamethylbenzene dication C$_6$(CH$_3$)$_6$$^{2+}$ shows a pentagonal-pyramidal structure involving a carbon-capped five-membered ring. The structural characterization of this hypercoordination (or hypervalency) gives rise if the aromatic behavior remains in the resulting pentagon ring. Here, we investigated the induced magnetic field of C$_6$(CH$_3$)$_6$$^{2+}$ to gain a deeper understanding of the resulting non-classical structural situation in a representative pentagonal-pyramidal structure. Our results support the view of a C$_5$(CH$_3$)$_5$$^−$/CCH$_3$$^{3+}$ structure, depicting a π-aromatic pentamethylcyclopentadienyl anion with a 6π-electron kernel, with a capped carbon which does not decrease the characteristic shielding cone property of the aromatic ring. Hence, carbon-capped rings are suggested to retain the aromatic behavior from the former aromatic ring. We expect that the analysis of both the overall magnetic response and NMR chemical shifts may be informative to unravel the characteristic patterns in the formation of hypervalent carbon atoms involving non-classical chemical environments.

Keywords: carbon; hypercoordination; aromaticity; shielding; DFT

1. Introduction

Carbon is a central element in organic chemistry, where the formation of fascinating non-classical species drives particular interest from the chemical community [1–3]. In such a field, the appearance of hypercoordinated (or hypervalent) carbon atoms [4–11] greatly expands the understanding of rules and criteria underlying the stability of certain structures.

Hypercoordination is common in heavier main group compounds, namely, PF$_5$ and SF$_6$, but is still very rare in carbon compounds owing to the usual four covalent bonds within octet rule restrictions. Recent characterization of penta- and hexa-coordinated carbocations from conclusive X-ray has provided further support to the long search for such groundbreaking species [12,13]. In particular, the crystal structure determination of the hexamethylbenzene dication C$_6$(CH$_3$)$_6$$^{2+}$ [13] settled previous assignations based on NMR spectroscopy among other experiments [14–16] of pentagonal-pyramidal dications.

An inherent and characteristic behavior of aromatic rings is that they are able to sustain a diamagnetic ring current along the structural backbone, which, in turn, leads to an induced magnetic field [17–20]. Such behavior is explained through the Pople ring current model [21], given the free π-electron precession under an applied field. The magnetic criteria of aromaticity [17,22–26] represent relevant probes widely employed in organic and inorganic species [19,22,23,27–29]. The use of single probes at the center of each structure has been discussed since its early introduction, being complemented with a global view given by the three-dimensional representation of both shielding and deshielding surfaces as fingerprint characteristics of aromatic species. For aromatic molecules, application

of a perpendicularly oriented external magnetic field ($\mathbf{B}^{ext}$) gives rise to an opposed induced field ($\mathbf{B}^{ind}$) which *shields* the former, which exhibits a long-range character with a complementary deshielding region at the molecular contour [19,20,26,30–32].

Moreover, ^{13}C-NMR studies have facilitated the determination of aromaticity from experiments in both solution and solid state, where atoms nearby aromatic units are shifted towards a shielding region [33–35]. In addition, in ^{13}C-NMR, the chemical shift anisotropy (CSA) pattern [36,37] of the non-aromatic C_{60} and hypothetical aromatic counterpart C_{60}^{10+} has been discussed previously, in order to account for the variation in aromaticity for sp^2 structural backbones, providing valuable information concerning the local properties at the nuclei, reflecting an axial symmetry for the aromatic carbon atoms [38].

Herein, we investigated the induced magnetic field and ^{13}C-NMR patterns of the hexamethylbenzene dication $C_6(CH_3)_6^{2+}$ [13], in order to gain a deeper understanding of the resulting situation in the characterized pentagonal-pyramidal structure bearing a representative hypercoordinated carbon atom.

2. Computational Details

Geometry optimizations and subsequent calculations were performed by using scalar relativistic DFT methods employing the ADF code [39] with the all-electron triple-ζ Slater basis set plus the double-polarization (STO-TZ2P) basis, in addition to the PBE0 functional [40–42]. The nuclear magnetic shielding tensors were calculated with the NMR module of ADF employing gauge-including atomic orbitals (GIAO) [31,43–45] with the exchange expression proposed by Handy and Cohen [46] and the correlation expression proposed by Perdew, Burke, and Ernzerhof [47] (OPBE), and the all-electron STO-TZ2P basis set. The information gained by $\mathbf{B}^{ind}$, given by the shielding tensor (σ) [30,31,48,49] according to $\mathbf{B}_{(r)}^{ind} = \sigma_{(r)}\mathbf{B}^{ext}$, can be generalized around the molecular domain, obtaining an overall representation of the magnetic response, which was obtained at several points of the molecular domain in a box of $30 \times 30 \times 30$ Borh^3 [50].

3. Results and Conclusion

The structure of the hexamethylbenzene dication $C_6(CH_3)_6^{2+}$ [13] is characterized by a pentagonal-pyramidal motif bearing a hypercoordinated carbon atom. The experimental structure [13] lies in a distorted C_5 axis with C−C bond lengths at the bottom C_5 ring in the range of 1.439(3)–1.445(2) Å, and 1.694(2)–1.715(3) Å for the C_5–CCH$_3$ bonds, leading to the formation of the pyramid. A distance from a C_5 centroid (point centered within the C_5 plane) to CCH$_3$ of 1.18 Å is found. The calculated structure (Figure 1) shows similar values, with a C_5 (centroid)–CCH$_3$ distance of 1.191 Å, and individual C_5–CCH$_3$ distances in the 1.712–1.724 Å range. The C_5 ring shows C–C bond lengths in the 1.451–1.455 Å range.

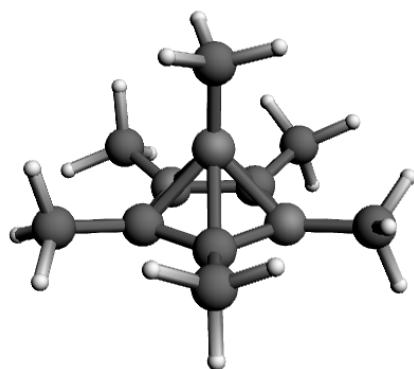**Figure 1.** Calculated structure for hexamethylbenzene dication $C_6(CH_3)_6^{2+}$.

The electronic structure was analyzed in terms of defined fragments accounting for the pentamethylcyclopentadienyl ($C_5(CH_3)_5^-$) motif, further coordinated with a CCH$_3^{3+}$ carbocation (Figure 2). Interestingly, the bonding features resemble the formation of

metallocenes [51], leading to the interaction of the π_1 and π_2,π_3 orbitals from the five-membered ring towards the σ and π orbital sets of the CCH_3^{3+} fragment. Hence, the formation of the pentagonal-pyramidal motif is rationalized as the bonding formation of one σ and two π bonds towards the CCH_3^{3+} carbocation. This molecular orbital interaction analysis supports the bonding elements discussed previously on the basis of the intrinsic bond orbital approach [52].
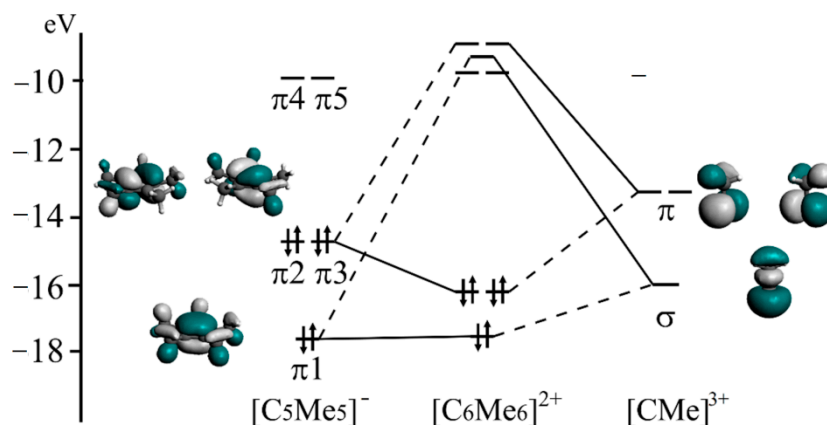

Figure 2. Formation of the electronic structure in terms denoting the combination of the set of π orbitals from $[C_5(CH_3)_5]^-$ and CCH_3^{3+} leading to the formation of both σ and π bonds.

The ^{13}C-NMR spectra depicted by Malischewski and Seppelt [13] show a peak at 125.5 ppm accounting for the C_5 ring atoms and at 8.2 ppm for the attached methyl groups, leaving signals at 21.0 ppm for the carbocation atom and at -4.5 ppm for the CCH_3 methyl group. The calculated (calc.) values are in agreement with the experimental (exp.) data (Table 1). Such values were compared to the calculated values for the isolated $C_5(CH_3)_5^-$ ring, with values of 99.3 ppm for C_5 ring atoms and 10.8 ppm for attached methyl groups, denoting that the latter groups remain similar upon the inclusion of the CCH_3 carbocation fragment, with a slight shielding (upfield) shift to 9.1 ppm. Ring atoms, in contrast, are consequently more affected, showing a deshielding (downfield) shift to 126.2 ppm (calc.) (125.3 ppm exp.) upon the formation of the pentagonal-pyramidal motif. For the carbocation atom and its attached methyl group, values amounting to 22.4 and -5.3 ppm were calculated, respectively.

Table 1. Calculated CSA parameters for different carbon atoms at $C_5(CH_3)_5^-$ and $C_6(CH_3)_6^{2+}$, accounting for the ^{13}C-NMR spectra. Values in ppm.

	σ_{11}	σ_{22}	σ_{33}	σ_{iso}	δ Shift	Exp. δ Shift [a]
$C_5(CH_3)_5^-$						
C_5 [b]	21.8	92.5	151.9	88.7	99.3	
CMe1 [b]	162.7	176.0	192.9	177.2	10.8	
$C_6(CH_3)_6^{2+}$						
C_5 [b]	−14.7	45.2	154.9	61.8	126.2	125.3
C [b]	130.1	136.2	230.5	165.6	22.4	21.0
CMe1 [b]	163.5	179.2	194.1	178.9	9.1	8.2
CMe2 [b]	184.1	184.5	211.4	193.3	−5.3	−4.5

[a] Experimental values taken from [13]. [b] C_5, carbon atoms at the C_5 ring; CMe1, methyl groups attached to C_5; C, carbocation; CMe2, methyl group attached to carbocation.

With the aim to exploit the information obtained from the chemical shift anisotropy (CSA) of the shielding tensor related to the chemical shift, we provide a graphical represen-

tation of the absolute shielding (σ_{ij}, i,j = 1, 2, 3), allowing to account for the orientation, magnitude, and sign of the local environment of the atom probe in relation to its own principal axis system (PAS) [31,53] (Figure 3). Usually, such relevant information is reduced to a single scalar value when the isotropic representation is employed, related to the regular solution state of magic-angle spinning solid-state measurements [54]. CSA is described in terms of the principal components of the shielding tensor given by $\sigma_{11} < \sigma_{22} < \sigma_{33}$, with σ_{33} as the most shielded component [55], enabling a clear analysis of the shielding tensor characteristics and their orientation.

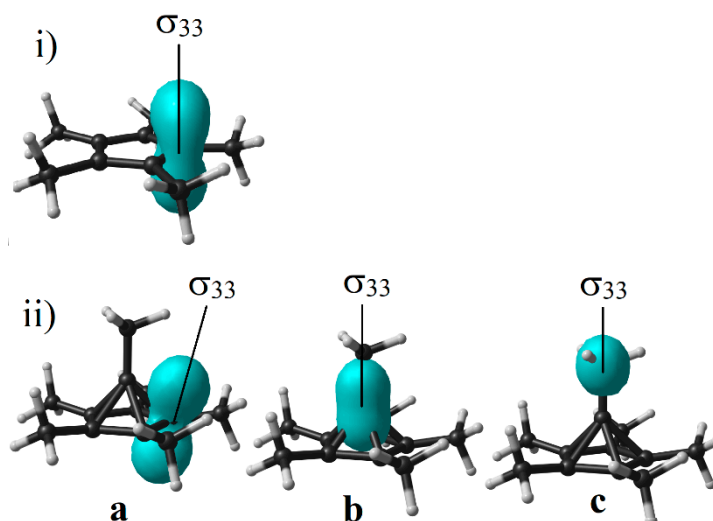**Figure 3.** Isosurface representation of nuclear shielding tensor for carbon atoms located at the C_5 ring in the $C_5(CH_3)_5{}^-$ fragment (**i**) and $C_6(CH_3)_6{}^{2+}$ (**ii,a**). In addition, the shapes of the shielding tensors located at the carbocation and attached methyl group atoms are presented in (**ii,b**) and (**ii,c**), respectively.

For the hexamethylbenzene dication $C_6(CH_3)_6{}^{2+}$ [13], the main shielding component (σ_{33}) of the C_5 ring atoms are oriented perpendicularly to the C_5 plane with a tilt angle of 14.1° (Supplementary Materials), which is in contrast to the uncoordinated $C_5(CH_3)_5{}^-$ ring, where it is oriented in a perfect perpendicular orientation (0°). For the carbocation atom and its attached methyl group, the σ_{33} component is oriented along the C_5 ring axis, also following the C–C bond axis.

The shielded value of the methyl group attached to the carbocation atom (CCH_3) with a value located at −4.5 ppm, in addition to the orientation of the shielded component of the CSA tensor [55], suggests the presence of a shielding region enabled by the bottom $C_5(CH_3)_5$ moiety. To further evaluate this point, we provide a graphical representation of the induced magnetic field under a field oriented perpendicular to the C_5 ring plane ($\mathbf{B}_z{}^{ind}$) in Figure 4, enabling the formation of the shielding cone property of aromatic rings, in agreement with the ring current effect established by Pople [21,26]. Such characteristics allow providing further validation of the aromatic behavior of the bottom C_5 ring within the hexamethylbenzene dication $C_6(CH_3)_6{}^{2+}$, favoring a description of the whole structure in terms of different fragments.

The obtained $\mathbf{B}_z{}^{ind}$ isosurface for $C_6(CH_3)_6{}^{2+}$ exhibits interesting features with a long-ranged shielding cone along the C_5 axis, complemented with a deshielding region lying at the C_5 plane. A shielding surface of 1 ppm is found at 7.0 Å from the center of the C_5 ring, whereas for the carbocation capped face, such surface is extended to 8.0 Å, owing to the contribution from the methyl group. The extension of a 3 ppm shielding surface is extended up to 4.4 Å for the uncapped side and 6.0 Å for the side incorporating the CCH_3 group. Noteworthy, such characteristics are strongly related to the isolated

pentamethyl-cyclopentadienyl anion (Cp*$^-$; $C_5(CH_3)_5{}^-$) featuring a 6π-electron kernel in a Húckel aromatic ring.

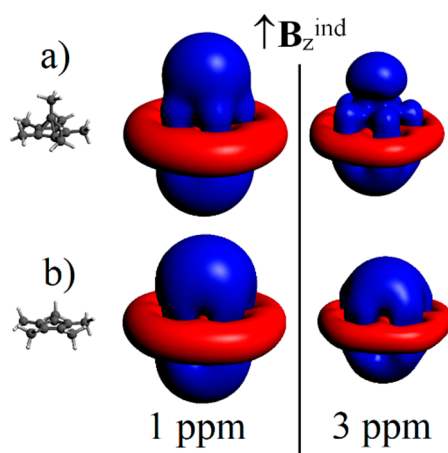**Figure 4.** $B_z{}^{ind}$ terms of the induced magnetic field for $C_6(CH_3)_6{}^{2+}$ (**a**) and $C_5(CH_3)_5{}^-$ (**b**), at 1 and 3 ppm. Blue: shielding; red: deshielding.

For $C_5(CH_3)_5{}^-$, the obtained $B_z{}^{ind}$ isosurface shows the expected shielding cone property related to planar aromatics, featuring a shielding surface of 1 ppm located at 7.0 Å from the center of the ring and of 3 ppm at 4.4 Å. These features are retained in the overall $C_6(CH_3)_6{}^{2+}$, which, in light of such findings, is composed of a 6π-aromatic ring provided by the bottom $C_5(CH_3)_5$ moiety under the magnetic criteria of aromaticity.

Such characteristics provide further validation of the structure of the hexamethyl-benzene dication $C_6(CH_3)_6{}^{2+}$ as being related to other organometallic half sandwich species [52], involving the bonding interaction between the 2s and 2p orbitals from the carbocation atom from the $CCH_3{}^{3+}$ fragment, and the set of π_1, π_2, and π_3 orbitals of the bottom $C_5(CH_3)_5$ moiety (see above). In agreement with previous discussions [52], the resulting aromatic character of the pentagonal-pyramid cage appears to be of planar aromatic, which was initially ascribed as a spherical aromatic structure owing to the close proximity of the NICS probe to the center of the $C_5(CH_3)_5{}^-$ ring.

To further address the shielding effect raised from the bottom aromatic $C_5(CH_3)_5{}^-$ ring and extended along the $CCH_3{}^{3+}$ fragment axis, it leads to the sizable shielding of the methyl carbon (Figure 5). From the contour plot of the $B_z{}^{ind}$ component, the resulting shielding region raised by the aromatic ring is reinforced by the C–C bond from $CCH_3{}^{3+}$, leading to an enhanced shielding region nearby the latter methyl group, accounting for the observed results at -4.5 ppm [13] (-5.3 ppm calc.).
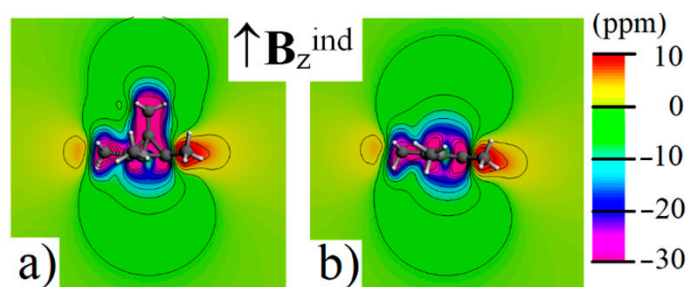

Figure 5. Contour plot representation of the $B_z{}^{ind}$ terms for the induced magnetic field for $C_6(CH_3)_6{}^{2+}$ (**a**) and $C_5(CH_3)_5{}^-$ (**b**).

4. Conclusions

In summary, the formation of the hexamethylbenzene dication $C_6(CH_3)_6^{2+}$ was discussed in terms of molecular orbital diagrams as a result of the bonding interaction between the 2s and 2p orbitals from the carbocation CCH_3^{3+} atom, and the set of π_1, π_2, and π_3 orbitals of the $C_5(CH_3)_5^-$ moiety. Such bonding features lead to a $C_5(CH_3)_5^- \rightarrow CCH_3^{3+}$ charge transfer, similar to half sandwich species.

The ^{13}C-NMR features a sizable downshift of the C_5 aromatic ring upon CCH_3^{3+} coordination. The rationalization as a $C_5(CH_3)_5^- - CCH_3^{3+}$ aggregate supports the formation of a planar aromatic ring being capped by the carbocation fragment. Analysis of both shielding/deshielding regions exposed the strong resemblance between $C_6(CH_3)_6^{2+}$ and the isolated $C_5(CH_3)_5^-$ anion (Cp^{*-}), owing to the related shielding cone property upon a perpendicularly applied external field.

Such description as a $C_5(CH_3)_5^- - CCH_3^{3+}$ interaction accounts for the observed shielding ^{13}C-NMR shift for the carbocation attached methyl group. We expect that the analysis of both the overall magnetic response and NMR local chemical shifts may be informative for unraveling the characteristic patterns in the formation of hypervalent carbon atoms involving non-classical chemical environments.

Supplementary Materials: The following are available online at https://www.mdpi.com/article/10.3390/chemistry3040097/s1, Figure S1: Determination of the tilt angle for the CSA tensor of a representative carbon atom at C_5 moiety in the $C_6(CH_3)_6^{2+}$ struc-ture. Red line shows a perfectly parallel orientation.

Author Contributions: Conceptualization, A.M.-C. and D.M.-C.; methodology, A.M.-C. and D.M.-C.; data curation, A.M.-C. and D.M.-C.; writing—review and editing, A.M.-C. and D.M.-C. All authors have read and agreed to the published version of the manuscript.

Data Availability Statement: The data presented in this study are available in Supplementary Material.

Conflicts of Interest: The authors declare no conflict of interest.

References

1. Minkin, V.I.; Minyaev, R.M.; Hoffmann, R. Non-classical structures of organic compounds: Unusual stereochemistry and hypercoordination. *Russ. Chem. Rev.* **2002**, *71*, 869–892. [CrossRef]
2. Hogeveen, H.; Kwant, P.W. Chemistry and spectroscopy in strongly acidic solutions. XL. $(CCH_3)_6^{2+}$, an unusual dication. *J. Am. Chem. Soc.* **1974**, *96*, 2208–2214. [CrossRef]
3. Hogeveen, H.; Kwant, P.W. Pyramidal mono- and dications. Bridge between organic and organometallic chemistry. *Accounts Chem. Res.* **1975**, *8*, 413–420. [CrossRef]
4. Jemmis, E.D.; Jayasree, E.G.; Parameswaran, P. Hypercarbons in polyhedral structures. *Chem. Soc. Rev.* **2006**, *35*, 157–168. [CrossRef]
5. Marx, D. CH_5^+: The cheshire cat smiles. *Science* **1999**, *284*, 59–61. [CrossRef]
6. Thompson, K.C.; Crittenden, D.L.; Jordan, M.J.T. CH_5^+: Chemistry's chameleon unmasked. *J. Am. Chem. Soc.* **2005**, *127*, 4954–4958. [CrossRef]
7. Vassilev-Galindo, V.; Pan, S.; Donald, K.J.; Merino, G. Planar pentacoordinate carbons. *Nat. Rev. Chem.* **2018**, *2*, 0114. [CrossRef]
8. Boldyrev, A.I.; Simons, J. Tetracoordinated planar carbon in pentaatomic molecules. *J. Am. Chem. Soc.* **1998**, *120*, 7967–7972. [CrossRef]
9. Heine, T.; Merino, G. What is the maximum coordination number in a planar structure? *Angew. Chem. Int. Ed.* **2012**, *51*, 4275–4276. [CrossRef] [PubMed]
10. Yañez, O.; Báez-Grez, R.; Garza, J.; Pan, S.; Barroso, J.; Vásquez-Espinal, A.; Merino, G.; Tiznado, W. Embedding a planar hypercoordinate carbon atom into a [4n+2] π-System. *ChemPhysChem* **2019**, *21*, 145–148. [CrossRef] [PubMed]
11. Trindle, C.; Altun, Z.; Bleda, E.A. Bonding analysis of compounds with unusual coordination of carbon: Proposed symmetric systems with six-coordinate carbon. *Molecule* **2020**, *25*, 3937. [CrossRef] [PubMed]
12. Scholz, F.; Himmel, D.; Heinemann, F.W.; Schleyer, P.V.R.; Meyer, K.; Krossing, I. Crystal structure determination of the nonclassical 2-norbornyl cation. *Science* **2013**, *341*, 62–64. [CrossRef] [PubMed]
13. Malischewski, M.; Seppelt, K. Crystal structure determination of the pentagonal-pyramidal hexamethylbenzene dication C_6 $(CH_3)_6^{2+}$. *Angew. Chem. Int. Ed.* **2017**, *56*, 368–370. [CrossRef] [PubMed]

14. Hogeveen, H.; Kwant, P.W. Direct observation of a remarkably stable dication of unusual structure: $(CCH_3)_6{}^{2\oplus}$. *Tetrahedron Lett.* **1973**, *14*, 1665–1670. [CrossRef]

15. Hogeveen, H.; Kwant, P.W.; Postma, J.; van Duynen, P.T. Electronic spectra of pyramidal dications, $(CCH_{36}{}^{2+}$ and $(CH)_6{}^{2+}$. *Tetrahedron Lett.* **1974**, *15*, 4351–4354. [CrossRef]

16. Hogeveen, H.; Van Kruchten, E.M.G.A. Isotopic perturbation of the carbon-13 nuclear magnetic resonance spectrum of a pyramidal dication. *J. Org. Chem.* **1981**, *46*, 1350–1353. [CrossRef]

17. Gershoni-Poranne, R.; Stanger, A. The NICS-XY-Scan: Identification of local and global ring currents in multi-ring systems. *Chem.-A Eur. J.* **2014**, *20*, 5673–5688. [CrossRef]

18. Steiner, E.; Fowler, P.W. Ring currents in aromatic hydrocarbons. *Int. J. Quantum Chem.* **1996**, *60*, 609–616. [CrossRef]

19. Islas, R.; Heine, T.; Merino, G. The induced magnetic field. *Acc. Chem. Res.* **2012**, *45*, 215–228. [CrossRef]

20. Merino, G.; Heine, T.; Seifert, G. The induced magnetic field in cyclic molecules. *Chem. -A Eur. J.* **2004**, *10*, 4367–4371. [CrossRef]

21. Pople, J.A.; Untch, K.G. Induced paramagnetic ring currents. *J. Am. Chem. Soc.* **1966**, *88*, 4811–4815. [CrossRef]

22. Gershoni-Poranne, R.; Stanger, A. Magnetic criteria of aromaticity. *Chem. Soc. Rev.* **2015**, *44*, 6597–6615. [CrossRef] [PubMed]

23. Benassi, R.; Lazzeretti, P.; Taddei, F. Magnetic criteria for aromaticity. *J. Phys. Chem.* **1975**, *79*, 848–851. [CrossRef]

24. Bird, C.W. The relationship of classical and magnetic criteria of aromaticity. *Tetrahedron* **1996**, *52*, 9945–9952. [CrossRef]

25. Steiner, E.; Fowler, P.W. On the orbital analysis of magnetic properties. *Phys. Chem. Chem. Phys.* **2004**, *6*, 261–272. [CrossRef]

26. Von Schleyer, P.R.; Jiao, H. What is aromaticity? *Pure Appl. Chem.* **1996**, *68*, 209–218. [CrossRef]

27. Kulichenko, M.; Fedik, N.; Boldyrev, A.; Muñoz-Castro, A. Expansion of magnetic aromaticity criteria to multilayer structures: Magnetic response and spherical aromaticity of matryoshka-like cluster $[Sn@Cu_{12}@Sn_{20}]^{12-}$. *Chem.-A Eur. J.* **2020**, *26*, 2263–2268. [CrossRef]

28. Furukawa, S.; Fujita, M.; Kanatomi, Y.; Minoura, M.; Hatanaka, M.; Morokuma, K.; Ishimura, K.; Saito, M. Double aromaticity arising from σ- and π-rings. *Commun. Chem.* **2018**, *1*, 60. [CrossRef]

29. Heine, T.; Islas, R.; Merino, G. σ and π contributions to the induced magnetic field: Indicators for the mobility of electrons in molecules. *J. Comput. Chem.* **2007**, *28*, 302–309. [CrossRef] [PubMed]

30. Lazzeretti, P. Assessment of aromaticity via molecular response properties. *Phys. Chem. Chem. Phys.* **2004**, *6*, 217–223. [CrossRef]

31. Kaupp, M.; Bühl, M.; Malkin, V.G. *Calculation of NMR and EPR Parameters: Theory and Applications*; John Wiley & Sons, Inc.: Hoboken, NJ, USA, 2006.

32. Papadopoulos, A.G.; Charistos, N.D.; Muñoz-Castro, A. Magnetic response of aromatic rings under rotation: Aromatic shielding cone of benzene upon different orientations of the magnetic field. *ChemPhysChem* **2017**, *18*, 1499–1502. [CrossRef]

33. Ehnbom, A.; Hall, M.B.; Gladysz, J.A. Origin of shielding and deshielding effects in NMR spectra of organic conjugated polyynes. *Org. Lett.* **2019**, *21*, 753–757. [CrossRef]

34. Vernet, R.D.; Boekelheide, V. Nuclear magnetic resonance spectroscopy. Ring-current effects on carbon-13 chemical shifts. *Proc. Natl. Acad. Sci. USA* **1974**, *71*, 2961–2964. [CrossRef] [PubMed]

35. Johnson, C.E.; Bovey, F.A. Calculation of nuclear magnetic resonance spectra of aromatic hydrocarbons. *J. Chem. Phys.* **1958**, *29*, 1012–1014. [CrossRef]

36. Yannoni, C.S.; Johnson, R.D.; Meijer, G.; Bethune, D.S.; Salem, J.R. Carbon-13 NMR study of the C60 cluster in the solid state: Molecular motion and carbon chemical shift anisotropy. *J. Phys. Chem.* **1991**, *95*, 9–10. [CrossRef]

37. Orendt, A.M.; Facelli, J.C.; Bai, S.; Rai, A.; Gossett, M.; Scott, L.T.; Boerio-Goates, J.; Pugmire, R.J.; Grant, D.M. Carbon-13 shift tensors in polycyclic aromatic compounds. 8.1a low-temperature NMR study of coronene and corannulene. *J. Phys. Chem. A* **2000**, *104*, 149–155. [CrossRef]

38. Muñoz-Castro, A. Axis-dependent magnetic behavior of C60and C6010+. consequences of spherical aromatic character. *Chem. Commun.* **2015**, *51*, 10287–10290. [CrossRef] [PubMed]

39. SCM. *ADF Code*; Vrije Universiteit: Amsterdam, The Netherlands, 2019. Available online: http://www.scm.com (accessed on 5 October 2021).

40. Becke, A.D. Density-functional exchange-energy approximation with correct asymptotic behavior. *Phys. Rev. A* **1988**, *38*, 3098–3100. [CrossRef]

41. Perdew, J.P. Density-functional approximation for the correlation energy of the inhomogeneous electron gas. *Phys. Rev. B* **1986**, *33*, 8822–8824. [CrossRef]

42. Adamo, C.; Barone, V. Toward reliable density functional methods without adjustable parameters: The PBE0 model. *J. Chem. Phys.* **1999**, *110*, 6158–6170. [CrossRef]

43. Wolinski, K.; Hinton, J.F.; Pulay, P. Efficient implementation of the gauge-independent atomic orbital method for NMR chemical shift calculations. *J. Am. Chem. Soc.* **1990**, *112*, 8251–8260. [CrossRef]

44. Schreckenbach, G.; Ziegler, T. Calculation of NMR shielding tensors using gauge-including atomic orbitals and modern density functional theory. *J. Phys. Chem.* **1995**, *99*, 606–611. [CrossRef]

45. Wolff, S.K.; Ziegler, T.; Van Lenthe, E.; Baerends, E.J. Density functional calculations of nuclear magnetic shieldings using the zeroth-order regular approximation (ZORA) for relativistic effects: ZORA nuclear magnetic resonance. *J. Chem. Phys.* **1999**, *110*, 7689–7698. [CrossRef]

46. Handy, N.C.; Cohen, A. Left-right correlation energy. *Mol. Phys.* **2001**, *99*, 403–412. [CrossRef]

47. Perdew, J.P.; Burke, K.; Ernzerhof, M. Generalized gradient approximation made simple. *Phys. Rev. Lett.* **1997**, *78*, 1396. [CrossRef]

48. Ziarelli, F.; Caldarelli, S. Solid-state NMR as an analytical tool: Quantitative aspects. *Solid State Nucl. Magn. Reson.* **2006**, *29*, 214–218. [CrossRef] [PubMed]

49. Heine, T.; Corminboeuf, C.; Seifert, G. The magnetic shielding function of molecules and pi-electron delocalization. *Chem. Rev.* **2005**, *105*, 3889–3910. [CrossRef] [PubMed]

50. Schleyer, P.V.R.; Maerker, C.; Dransfeld, A.; Jiao, H.; van Eikema Hommes, N.J. Nucleus-independent chemical shifts: A simple and efficient aromaticity probe. *J. Am. Chem. Soc.* **1996**, *118*, 6317–6318. [CrossRef]

51. Cotton, F. *Chemical Applications of Group Theory*; Wiley-Interscience: Hoboken, NJ, USA, 1990.

52. Klein, J.E.M.N.; Havenith, R.W.A.; Knizia, G. The pentagonal-pyramidal hexamethylbenzene dication: Many shades of coordination chemistry at Carbon. *Chem. -A Eur. J.* **2018**, *24*, 12340–12345. [CrossRef]

53. Kaupp, M. Interpretation of NMR chemical shifts. In *Calculation of NMR and EPR Parameters*; Wiley-VCH Verlag GmbH {&} Co. KGaA: Weinheim, Germany, 2004; pp. 293–306. [CrossRef]

54. Chan, J.C.C. Solid state NMR. In *Topics in Current Chemistry*; Springer: Berlin/Heidelberg, Germany, 2012; Volume 306, ISBN 978-3-642-24802-3.

55. Haeberlen, U. High resolution Nmr in solids: Selective averaging. In *Advances Hin Magnetich Resolution Nmr in Solids Selective Averaginceg*; Academic Press: New York, NY, USA, 1976.